Lysosomal degradation of endocytosed proteins depends on the chloride transport protein ClC-7

Lena Wartosch,*,† Jens C. Fuhrmann,*,1 Michaela Schweizer,‡ Tobias Stauber,* and Thomas J. Jentsch*,2

*Leibniz-Institut für Molekulare Pharmakologie (FMP) and Max-Delbrück-Centrum für Molekulare Medizin (MDC), Berlin, Germany; †Freie Universität, Berlin, Germany; and ‡Zentrum für Molekulare Neurobiologie (ZMNH), Universität Hamburg, Hamburg, Germany

ABSTRACT   Mutations in either ClC-7, a late endosomal/lysosomal member of the CLC family of chloride channels and transporters, or in its β-subunit Ostm1 cause osteopetrosis and lysosomal storage disease in mice and humans. The severe phenotype of mice globally deleted for ClC-7 or Ostm1 and the absence of storage material in cultured cells hampered investigations of the mechanism leading to lysosomal pathology in the absence of functional ClC-7/Ostm1 transporters. Tissue-specific ClC-7-knockout mice now reveal that accumulation of storage material occurs cell-autonomously in neurons or renal proximal tubular cells lacking ClC-7. Almost all ClC-7-deficient neurons die. The activation of glia is restricted to brain regions where ClC-7 has been inactivated. The effect of ClC-7 disruption on lysosomal function was investigated in renal proximal tubular cells, which display high endocytotic activity. Pulse-chase endocytosis experiments *in vivo* with mice carrying chimeric deletion of ClC-7 in proximal tubules allowed a direct comparison of the handling of endocytosed protein between cells expressing or lacking ClC-7. Whereas protein was endocytosed similarly in cells of either genotype, its half-life increased significantly in ClC-7-deficient cells. These experiments demonstrate that lysosomal pathology is a cell-autonomous consequence of ClC-7 disruption and that ClC-7 is important for lysosomal protein degradation.—Wartosch, L., Fuhrmann, J. C., Schweizer, M., Stauber, T., Jentsch, T. J. Lysosomal degradation of endocytosed proteins depends on the chloride transport protein ClC-7. *FASEB J.* 23, 000–000 (2009). www.fasebj.org

CLC-7 IS A UBIQUITOUSLY EXPRESSED member of the CLC gene family of Cl^- channels and Cl^-/H^+ exchangers (1). Of the 9 mammalian CLC proteins, 4 members are plasma membrane Cl^- channels, whereas others, including ClC-7, are sited predominantly in membranes of the endolysosomal pathway (2). The presence of a certain "proton glutamate" in ClC-3 through ClC-7 suggested that ClC-7 functions as a

Cl^-/H^+ exchanger, in analogy to the bacterial EcClC-1 (3) and mammalian ClC-4 and ClC-5 proteins (4, 5). Indeed lysosomes, which prominently express ClC-7 and its β-subunit Ostm1 (6–8), show Cl^-/H^+-exchange activity (9). ClC-7/Ostm1 is also found on late endosomes and a specialized acid-secreting plasma membrane domain of osteoclasts (6–8). The latter membrane ("ruffled border") is believed to be formed by lysosomal exocytosis.

Compartments of the endocytic pathway are progressively acidified along their way from the plasma membrane to the lysosome. Their low luminal pH is important for such processes as receptor-ligand interaction, endolysosomal trafficking, and luminal enzymatic activity (10), rendering it a key parameter for processing and degradation of endocytosed material. The active accumulation of protons is achieved mainly through V-type H^+-ATPases that act as electrogenic proton pumps. Intracellular CLC proteins are thought to facilitate endosomal/lysosomal acidification by providing an electrical shunt for proton pumping (2).

Disruption of specific vesicular CLC proteins has diverse effects, such as impaired renal endocytosis and kidney stone formation with a loss of ClC-5 (11–13) or neurodegeneration with the loss of ClC-3 (14). The loss of either ClC-7 (7) or its β-subunit Ostm1 (8, 15) leads to excessive bone mineralization (osteopetrosis) and to a severe degeneration of the brain and retina (6–8). The neurodegeneration observed in mice lacking either ClC-7 or Ostm1 displays typical features of human neuronal ceroid lipofuscinosis (NCL), a neurodegenerative lysosomal storage disease (6, 8). Neurological abnormalities and blindness have also been described in osteopetrotic patients carrying mutations in *CLCN7* (16) or *OSTM1* on both alleles (17). In $Clcn7^{-/-}$ mice, the accumulation of lysosomal storage material in neuronal cell bodies precedes neuronal cell loss that is

---

evident as early as 30 d after birth (P30) (6). The exact mechanism for lysosomal deposition with a loss of ClC-7/Ostm1 activity is unknown. Neither lysosomal pH nor the activity of the lysosomal enzyme tripeptidylpeptidase I (TPP I) were altered in cultured ClC-7-deficient neurons or fibroblasts (6). The short life span and complex phenotype of constitutive ClC-7-knockout (KO) mice (6, 7) was a severe obstacle in the analysis of lysosomal function *in vivo* and prevented us from following the progression of neurodegeneration.

Newly generated conditional KO mice now reveal that accumulation of lysosomal storage material is intrinsic to cells lacking ClC-7. The massive activation of microglia and astrocytes is limited to brain regions where ClC-7 has been deleted. Chimeric deletion of ClC-7 in proximal tubular cells (PTCs) enabled us to compare directly the uptake and degradation of proteins between cells of either genotype. We show that ClC-7 is important for the lysosomal degradation of proteins but not for their endocytotic uptake.

MATERIALS AND METHODS

Mice

To generate "floxed" ClC-7 mice, a part of the murine ClC-7 gene (*Clcn7*), extending from the intron preceding exon 6 to the intron after exon 16, was cloned into a pKO Scrambler plasmid (Lexicon Genetics Incorporated, Woodland, TX, USA). A loxP site with a 5′ *Eco*RI site was introduced in the intron upstream of exon 12, a neomycin resistance (neo) cassette flanked by loxP sites behind exon 13, and a diphtheria toxin A cassette at the 5′ end of the targeting construct (Supplemental Fig. 1*A*). The vector was electroporated into R1 embryonal stem cells, and clones were tested for homologous recombination by Southern blot analysis (Supplemental Fig. 1*B*). After transfection with a plasmid expressing Cre recombinase, clones were tested for removal of the neo cassette by Southern blotting (Supplemental Fig. 1*C*). C57BL/6 blastocysts injected with correctly targeted cells were implanted into foster mothers. Male chimeras were bred with C57BL/6 females to yield heterozygous floxed ClC-7 mice ($Clcn7^{+/lox}$).

Forebrain-specific ClC-7-KO mice were obtained by crossing $Clcn7^{lox/lox}$ mice with mice (in a mixed C57BL/6-129/SVJ background) expressing Cre recombinase under control of the EMX1 promotor (18), mice with partial ClC-7 deletion in proximal tubules (PTs) by crossing $Clcn7^{lox/lox}$ mice with ApoE-cre mice (19) and backcrossing into C57BL/6 for ≥5 generations. In all experiments, wild-type (WT; $Clcn7^{+/+}$), $Clcn7^{+/lox}$, $Clcn7^{lox/lox}$, $Clcn7^{+/lox};cre$, or $Clcn7^{+/+};cre$ littermates served as controls.

$Clcn7^{-/-}$ and $Clcn5^{-/-}$ mice were described previously (7, 11). *Deleter*-Cre mice (20) were provided by Ralf Kühn (Helmholtz Zentrum München, Munich, Germany), EMX1-Cre mice (18) by Takuji Iwasato and Shigeyoshi Itohara (Brain Science Institute, RIKEN, Saitama, Japan), and ApoE-Cre mice (19) by Thomas Willnow (MDC, Berlin, Germany). All experiments conformed to the animal protection laws of Germany.

Histology and immunohistochemistry

Primary antibodies used were own KO-controlled rabbit anti-ClC-7 (7), guinea-pig anti-ClC-7 (8), rabbit anti-Ostm1 (8), rabbit anti-ClC-5 (21), rabbit anti-ClC-3 (22), mouse anti-lysobisphosphatidic acid (LBPA; ref. 23), rat anti-lysosome-associated membrane protein-1 (lamp-1; clone 1D4B; BD Pharmingen, Heidelberg, Germany), mouse anti-villin (Acris, Hiddenhausen, Germany), mouse anti-parvalbumin (Swant, Bellinzona, Switzerland), mouse anti-NeuN (Chemicon, Temeculla, CA, USA), rabbit anti-IBA1 (Wako Chemicals, Richmond, VA, USA), and mouse anti-glial fibrillary acidic protein (GFAP; Sigma, Deisenhofen, Germany). Secondary antibodies conjugated to Alexa Fluor 488, 546, or 633 (Molecular Probes, Karlsruhe, Germany) or horseradish peroxidase (HRP; Dianova, Hamburg, Germany) were used.

HRP was detected by incubation in solution containing 0.05% (w/v) 3,3′-diaminobenzidine (DAB), 0.03% (w/v) H_2O_2, and 0.04% nickel ammonium sulfate in 0.01 M phosphate buffer (PB). Endogenous peroxidase was exhausted by preincubation for 30 min in 0.3% H_2O_2 in 0.1 M PB. GSA-biotin (*Griffonia simplicifolia* agglutinin; Vector Laboratories, Burlingame, CA, USA) was detected using Streptavidin-Cy3 (Molecular Probes, Karlsruhe, Germany).

Perfusion of deeply anesthetized mice, fixation, and preparation of tissue and staining procedures were performed as described previously (6). For alkaline phosphatase-staining the Sigma Fast™ Fast Red TR/Naphtol AS-MX substrate kit (Sigma) was used according to the manufacturer's instructions.

Electron microscopy procedures were described previously (6). For semithin sections, tissues were sliced to 0.7 μm and stained with 0.1% (w/v) toluidine blue.

In vivo endocytosis of protein

Bovine β-lactoglobulin (L3908; Sigma) was labeled with either Alexa Fluor 546 or 700 succinimidyl esters (Molecular Probes). Dye solution in DMSO (50 μl of 10 mg/ml) was mixed with 1 ml β-lactoglobulin in PBS (10 mg/ml) and incubated under stirring for 1.5 h at RT in the dark. Uncoupled dye was removed by passing through Sephadex™ G-25 PD10 (GE Healthcare, Freiburg, Germany).

Mice were injected with labeled β-lactoglobulin (5 μg/g body weight for kidney-specific ClC-7-KO mice, 20 μg/g for ClC-7/ClC-5 double-KO mice) or with HRP type VI (300 μg/g) (Sigma) in PBS into the tail vein. Mice were anesthetized and perfused transcardially for 3 min using either PBS with 0.01% (w/v) heparin alone (for tissue lysates) or followed by 4% (w/v) PFA in PBS (immunohistochemistry).

Quantification of protein degradation

Mice were injected with β-lactoglobulin Alexa Fluor 546 and fixed as described above. After immunostaining kidney sections for ClC-7 and villin, images were acquired with an SP2 confocal microscope equipped with an ×40 1.25-NA oil-immersion lens (Leica, Mannheim, Germany). Imaging settings for the β-lactoglobulin Alexa Fluor 546 recording were identical for all tubules of the same time point. Fluorescence was quantified using the program NIH ImageJ 1.34 (http://rsbweb.nih.gov/ij/). In a chimeric PT, a region of interest (ROI) was drawn around ClC-7-expressing and -deficient PT areas, respectively, including the villin-stained brush border. For each tubule, the fluorescence intensity of β-lactoglobulin Alexa Fluor 546 was measured for the same number of WT and ClC-7-KO ROIs and the mean intensity was calculated. Background fluorescence was determined by measuring ROIs in the basal region of PTs fixed 10 min after injection, when those regions are clear of endocytosed protein. The averaged background fluorescence of 5 PTs was subtracted from the β-lactoglobulin Alexa Fluor 546 fluorescence in WT and

ClC-7-KO cells, respectively. For each PT, the ratio of the corrected WT and ClC-7-KO β-lactoglobulin fluorescence was calculated. Three independent experiments were performed, and more than 20 chimeric PTs per time point and animal were analyzed. Statistical differences were calculated with a Student's t test for paired data.

SDS-PAGE and immunoblot

Tissue homogenate preparation and immunoblots were performed as described previously (6). Equal amounts of protein were separated by SDS-PAGE using 4–12% NuPage® gradient bis-Tris gels in NuPage MES buffer (Invitrogen, Karlsruhe, Germany). β-lactoglobulin Alexa Fluor 700 was detected using a LI-COR® Odyssey fluorescent reader (LI-COR Biosciences, Bad Homburg, Germany) at 680-nm excitation and 780-nm emission wavelengths. For immunoblots, anti-α-tubulin, anti-actin (both Sigma), anti-LC3 (AP1802a; Abgent, San Diego, CA, USA), anti-ClC-7 (7), anti-ClC-3 (22), anti-ClC-5 (11), anti-Lamp-1 (BD Pharmingen) primary antibodies, and HRP-conjugated secondary antibodies (Dianova) were used.

RESULTS

Neurodegeneration in mice with forebrain-specific ClC-7 deletion

To inactivate ClC-7 in a tissue-specific manner, we generated mice in which exons 12 and 13 of the *Clcn7* gene are flanked by loxP sites (Supplemental Fig. 1). Mice homozygous for the floxed *Clcn7* allele exhibited normal levels of the ClC-7 protein (Supplemental Fig. 2*A*) and did not display any obvious phenotype regarding size, weight, or bone density (Supplemental Fig. 2*B*). Cre-mediated excision of *Clcn7* exons 12 and 13 leads to a premature stop codon in exon 14, within helix I of the trans-membrane domain. A truncated amino-terminal portion of ClC-7 could not be detected (data not shown), owed to either nonsense-mediated RNA decay or protein instability. Ubiquitous deletion of the floxed *Clcn7* allele by crossing *Clcn7*$^{lox/lox}$ mice with the *deleter* strain (20) produced the same phenotype as the constitutive ClC-7 KO (7), including severe osteopetrosis (Supplemental Fig. 2*C*).

We first crossed floxed ClC-7 mice with the EMX1-cre strain (18). This strain expresses Cre recombinase mainly in the hippocampus and cortical structures of the forebrain (18), as confirmed by reporter gene analysis (**Fig. 1***A*). The forebrain-restricted ClC-7 deletion was visualized by the reduction of ClC-7 immunoreactivity in the cortex and hippocampus (Fig. 1*B, C* and Supplemental Fig. 3*A*). In other brain regions, *e.g.*, the cerebellum, ClC-7 levels appeared unchanged (Fig. 1*C* and Supplemental Fig. 3*C*). ClC-7 deletion in cortex and hippocampus was incomplete because parvalbumin-positive, inhibitory neurons of the cortex and hippocampus still expressed ClC-7 (Supplemental Fig. 3*B*). This finding agrees with the predominant expression of Cre recombinase in excitatory neurons of the forebrain in EMX1-cre mice (18).

Forebrain-specific ClC-7-KO mice lived to the same age as WT littermates. They neither differed in size nor showed any sign of osteopetrosis (data not shown). Neurological abnormalities such as hind-limb clasping became apparent at the age of 4–5 mo (data not shown). At the same time, KO mice displayed a drastic reduction of the cortex (Fig. 1*D–I*). Nissl-stained sagittal brain sections revealed a massive loss of cortical neurons (Fig. 1*E, H*). In contrast, regions in which ClC-7 was not deleted (such as the cerebellum) were spared from neurodegeneration. Additionally, an enormous expansion of the lateral ventricle became obvious (Fig. 1*H, I*). An incipient hippocampal degeneration had been observed in constitutive ClC-7-KO mice around P30 but could not be followed much further because of the early death of those animals (6). At 1.5 yr of age, the cortex and hippocampus of forebrain-specific ClC-7-KO mice had almost disappeared (Fig. 1*F, I*), and semithin sections revealed a nearly complete loss of all cortical neurons in 1-yr-old forebrain-specific ClC-7-KO mice (Supplemental Fig. 4). The progressive degeneration of the hippocampus was followed by hematoxylin-eosin staining (Fig. 1*J–O*). Consistent with our previous results (6), neurodegeneration started in the CA3 region of the hippocampus, which showed severe neuronal cell loss as early as 30 d after birth (Fig. 1*J, M*). In 20-wk-old KO mice, the dentate gyrus showed conspicuous degeneration (Fig. 1*K, N*), and at 1.5 yr of age, hippocampal structures were no longer detectable (Fig. 1*L, O*).

Lysosomal storage disease entails region-restricted glia activation

Constitutive ClC-7-KO mice show an accumulation of electron-dense, osmiophilic lysosomal storage material in hippocampal and cortical neurons (6). These deposits, which display typical features of NCL, became apparent at 11 d after birth and increased with age (6). Electron microscopy on forebrain-specific ClC-7-KO mice revealed that prominent storage material was distributed throughout the somata of cortical neurons at P37 (**Fig. 2***A*) and at the age of 8 wk (data not shown). Immunoblotting brain lysates for LC3 showed a strong increase of the LC3-II form in constitutive ClC-7-KO mice (Fig. 2*B*), indicating an increase in autophagy (24).

A hallmark of NCL and of other neurodegenerative central nervous system (CNS) pathologies is astrogliosis and activation of microglia. Both features were observed in constitutive *Clcn7*$^{-/-}$ mice (6). We now show that these pathological changes are restricted to regions displaying lysosomal storage and neurodegeneration (**Fig. 3**). In forebrain-specific ClC-7-KO mice, astrogliosis and microglia activation appeared at first in the region of the hippocampus (Fig. 3*A*) from where it then spread over the cortex (Fig. 3*B* and Supplemental Fig. 5*A, B*). Immunofluorescence staining shows that activated, enlarged microglia express ClC-7 (Fig. 3*B*). Differences in the depicted microglia morphology between forebrain-specific and complete ClC-7-KO mice
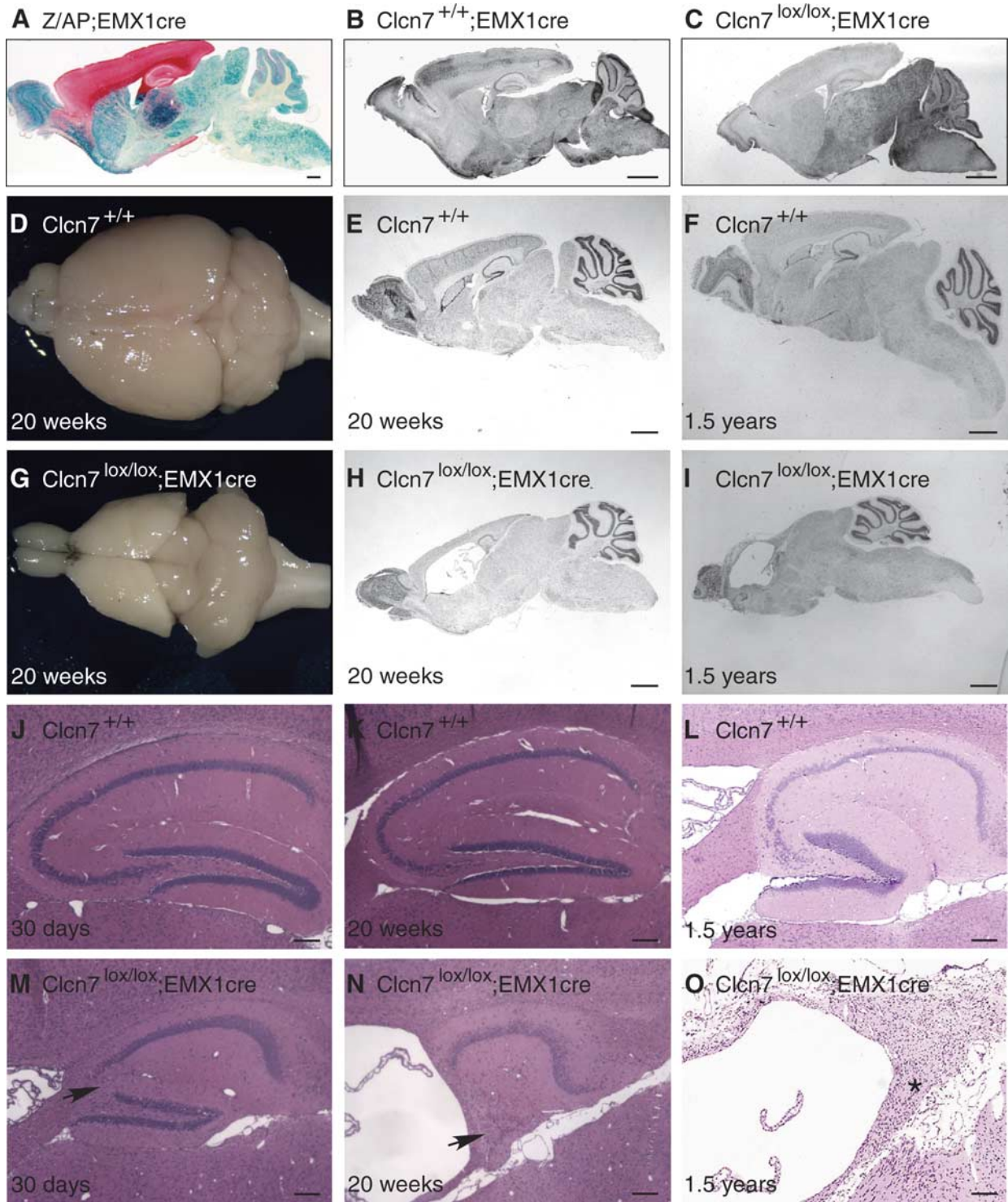
Figure 1. Neurodegeneration in forebrain-specific ClC-7-KO mice. *A*) Cre expression in the EMX1-cre mice crossed with the Z/AP reporter strain. Cre-expressing cells were stained red due to the expression of alkaline phosphatase. Cre-negative cells were stained blue by the activity of β-galactosidase. *B, C*) Antibody detection of ClC-7 using diaminobenzidine on brain slices of 2-wk-old control mice (*Clcn7*$^{+/+}$*;EMX1cre*) (*B*) and *Clcn7*$^{lox/lox}$*;EMX1cre* mice (*C*) showed deletion of ClC-7 in the cortex and hippocampus of forebrain-specific KO mice. *D–I*) Conspicuous loss of cortical and hippocampal neurons in whole-brain (*D, G*) or Nissl-stained sagittal brain sections of 20-wk-old (*E, H*) and 1.5-yr-old *Clcn7*$^{lox/lox}$*;EMX1cre* mice (*F, I*). *J–O*) Hematoxylin-eosin staining on sagittal brain sections in the hippocampal region in WT (*J–L*) and *Clcn7*$^{lox/lox}$*;EMX1cre* (*M–O*) mice. Neuronal loss in forebrain-specific ClC-7-KO mice started in the hippocampal CA3 region (*M*, arrow) and later extended to the dentate gyrus (*N*, arrow). No hippocampal structures could be detected in *Clcn7*$^{lox/lox}$*;EMX1cre* mice at 1.5 yr of age (*O*, asterisk). Scale bars = 2 mm (*A–C, E, F, H, I*); 200 μm (*J–O*).
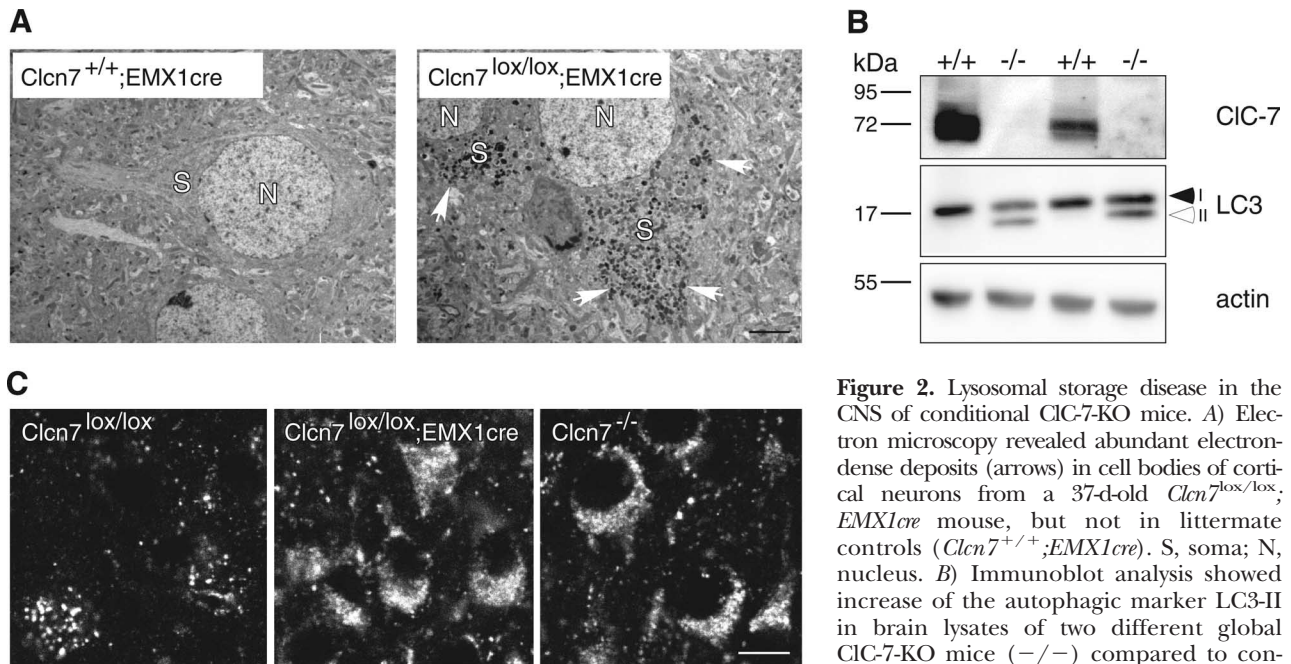
Figure 2. Lysosomal storage disease in the CNS of conditional ClC-7-KO mice. *A*) Electron microscopy revealed abundant electron-dense deposits (arrows) in cell bodies of cortical neurons from a 37-d-old *Clcn7*$^{lox/lox}$; *EMX1cre* mouse, but not in littermate controls (*Clcn7*$^{+/+}$;*EMX1cre*). S, soma; N, nucleus. *B*) Immunoblot analysis showed increase of the autophagic marker LC3-II in brain lysates of two different global ClC-7-KO mice ($-/-$) compared to controls ($+/+$) (age: 3–4 wk). *C*) Immunostaining against lamp-1 showed a typical punctate pattern in cortical neurons of control mice (*Clcn7*$^{lox/lox}$). Staining was more diffuse and more intense in cortical neurons of forebrain-specific ClC-7-KO mice (*Clcn7*$^{lox/lox}$;*EMX1cre*) and in the global KO (*Clcn7*$^{-/-}$) (P38). Scale bars = 3 μm (*A*); 15 μm (*C*).

are likely due to the different ages. No astrogliosis or microglia activation was found in regions with unaltered ClC-7 expression, such as the cerebellum (Supplemental Fig. 5*B*).

ClC-7-KO mice also displayed changed intraneuronal distribution of lamp-1, a marker of late endosomes and lysosomes (6). Constitutive and forebrain-specific ClC-7-KO mice showed a more diffuse and more intense staining in hippocampal (Supplemental Fig. 6) and cortical (Fig. 2*C*) neurons when compared to the punctate pattern in control (*Clcn7*$^{lox/lox}$) mice of the same age (P38).

Endosomal and lysosomal compartments in ClC-7-KO kidney cells

To understand processes underlying the lysosomal dysfunction of ClC-7-deficient cells more thoroughly, we investigated renal PTCs. These cells take up large amounts of protein, which is destined for lysosomal degradation. Considerable amounts of lysosomal storage material accumulate in renal PTCs of *Clcn7*$^{-/-}$ and *Ostm1*$^{-/-}$ mice (6, 8) and, as observed in the brain (Fig. 2*B*), kidney tissue displayed increased amounts of the autophagy marker LC3-II (Supplemental Fig. 7*A*).

ClC-7 is strongly expressed in the kidney (1). To investigate the renal expression pattern of ClC-7 more precisely, we made use of mice that express a ClC-7/lacZ fusion protein (7). Analysis of X-Gal-stained kidneys from these mice revealed a broad expression of ClC-7 in all parts of the kidney (Supplemental Fig. 7*B*). Immunohistochemistry of WT renal cortex (**Fig. 4***A*)

revealed that ClC-7 is most strongly expressed in PTCs, which were identified by costaining for the brush-border protein villin. Prominent staining for ClC-7 was also detected in other nephron segments, such as the cortical collecting duct and thick ascending limb (both identified by the presence of barttin; ref. 25), as well as in podocytes of glomeruli. In the PTCs, we compared the subcellular localization of ClC-7 to those of ClC-3 and ClC-5, both of which are expressed in this nephron segment and which reside on distinct endosomal compartments (14, 21, 22, 26). When investigated by immunofluorescence, neither protein showed a significant overlap with ClC-7 (Fig. 4*B*, *C*). In contrast to ClC-7-positive late endosomes/lysosomes, endosomes containing ClC-5 or ClC-3 are located more apically, in closer proximity to the brush border.

As in other cell types (6–8), ClC-7 colocalizes with its β-subunit Ostm1 (Supplemental Fig. 7*C*) and lamp-1 (**Fig. 5***A*) on subapical structures in PTCs. Because ClC-7 and Ostm1 are only stable when forming ClC-7/Ostm1 heteromers (8), Ostm1 was undetectable in ClC-7-deficient PTCs (Supplemental Fig. 8*B*). In PTCs of ClC-7-KO and Ostm1-deficient *gray lethal* mice, lamp-1-positive structures were drastically enlarged and distributed over a much broader area of the cell (Fig. 5*A* and Supplemental Fig. 7*D*). This pattern resembles the diffuse lamp-1 pattern in *Clcn7*$^{-/-}$ neurons (Fig. 2*C* and Supplemental Fig. 6). We asked whether the subcellular distribution of earlier parts of the endolysosomal pathway were altered in ClC-7-deficient PTCs and investigated the localization of ClC-5 and ClC-3. Costaining with lamp-1 on ClC-7-deficient PTCs did not reveal any
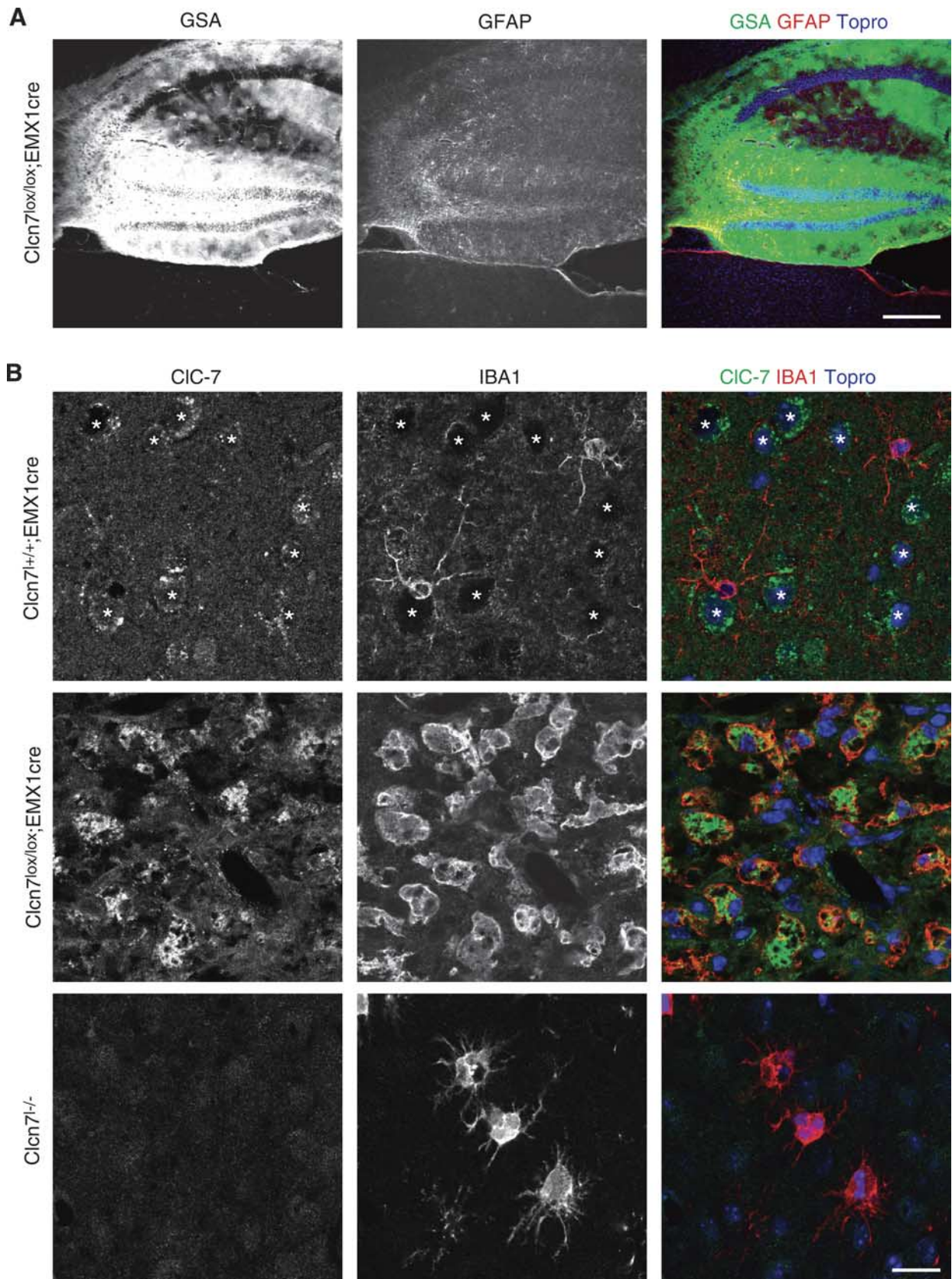
Figure 3. Activation of astrocytes and microgliosis in forebrain-specific ClC-7-KO mice. Brain sections stained with a microglia-binding lectin (GSA) and with an antibody against GFAP (staining astrocytes) (*A*) or with antibodies against ClC-7 and the microglia marker protein IBA1 (*B*). *A*) Massive activation of microglia and astrocytes in the hippocampus of 31-d-old $Clcn7^{\text{lox/lox}};EMX1cre$ mice. *B*) ClC-7 is expressed in cortical neurons (asterisks) of control ($Clcn7^{+/+};EMX1cre$) mice. Microglia are activated in the cortex of 46-d-old $Clcn7^{\text{lox/lox}};EMX1cre$ mice and strongly express ClC-7. No ClC-7 signal was detected in activated microglia of globally-deleted $Clcn7^{-/-}$ mice (age P31). Scale bars = 300 μm (*A*); 40 μm (*B*).
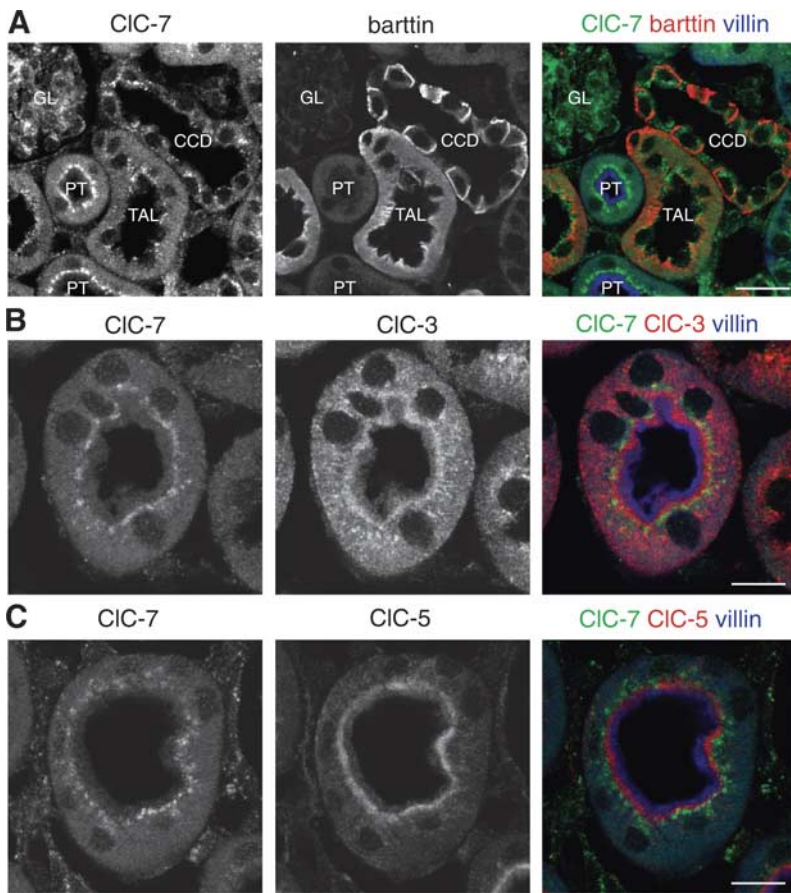
Figure 4. Expression of ClC-7 in the kidney. *A*) Staining with antibodies against ClC-7 (green), barttin (red), and villin (blue) revealed ClC-7 expression in different cortical nephron segments, such as proximal tubules (PT), cortical collecting duct (CCD), and thick ascending limb (TAL), and in podocytes of the glomerulus (GL). *B, C*) A limited overlap exists between ClC-7 and ClC-3 signals (*B*). The majority of ClC-7-positive late endosomes and lysosomes are distinct from the more apical ClC-3-positive (*B*) and ClC-5-positive (*C*) compartments (endosomes). Scale bars = 40 μm (*A*); 15 μm (*B, C*).

major changes in morphology and distribution of either ClC-5-positive (early) or ClC-3-positive (late) endosomes (Fig. 5*B, C*). Neither did we find altered expression levels of ClC-3, ClC-5, or lamp-1 in immunoblot analysis of kidney tissue (Supplemental Fig. 7*E*).

We next asked whether the enlarged lamp-1-positive structures in ClC-7-KO PTCs are integral parts of the endocytic system. We performed *in vivo* pulse-chase experiments in which we injected intravenously the low-molecular-weight (18 kDa) protein β-lactoglobulin that is endocytosed from the primary urine by PTCs (11). At 1 h after injection, fluorescently labeled β-lactoglobulin was found in lumina of enlarged lamp-1-positive compartments of ClC-7-deficient PTCs (**Fig. 6***A*), demonstrating that these structures are connected to the endocytic system. The presence of LBPA on these structures (Fig. 6*B*) strongly suggests that these vesicles share features with multivesicular endosomes (23) rather than being solely of lysosomal nature.

Slower protein degradation in ClC-7-KO mice

To study the uptake and degradation of endocytosed proteins in WT and ClC-7-KO PTCs under identical conditions, we investigated PTs that contain cells expressing or lacking ClC-7 side by side. To this end, we crossed our floxed ClC-7 mouse with mice that express Cre recombinase under a renal cortex-specific ApoE promotor element, which, however, is not active in every PTC (19).

We first examined lamp-1 expression in those chimeric tubules. Only cells lacking ClC-7, but not neighboring WT cells, displayed enlarged lamp-1-positive structures (**Fig. 7***A*). Hence, the enlargement of lamp-1-positive structures is a cell-autonomous effect of ClC-7 deletion. We next attempted to test whether this phenotype might be rescued by a reduction in endocytic uptake. To this end, we crossed the kidney-specific ClC-7-KO mice to ClC-5-KO mice (11), which exhibit drastically reduced endocytosis in PTCs (11, 13). Lamp-1-positive structures appeared unaltered in PTCs lacking only ClC-5 (Supplemental Fig. 8*C*). No discernible effect of ClC-5 absence on the ClC-7-KO-induced altered distribution and size of lamp-1-positive structures was observed in PTs that were chimeric for ClC-5 due to random X-chromosomal inactivation (Fig. 7*B*).

After chasing endocytosed protein for 1 h into PT lysosomes of kidney-specific ClC-7-KO mice, KO cells displayed much stronger fluorescence of labeled β-lactoglobulin than neighboring WT cells of the same tubule (**Fig. 8***A* and Supplemental Fig. 8*A, B*). The stronger accumulation of β-lactoglobulin in ClC-7-KO cells might be explained either by increased endocytosis or by impaired protein degradation. To distinguish between these possibilities, we performed pulse-chase endocytosis experiments. Fluorescence of labeled β-lactoglobulin was quantified for PT sections expressing or lacking ClC-7 (Fig. 8*A, B*). At 10 min after injection, β-lactoglobulin fluorescence did not differ between WT and KO cells. Hence, ClC-7 disruption has no appre-
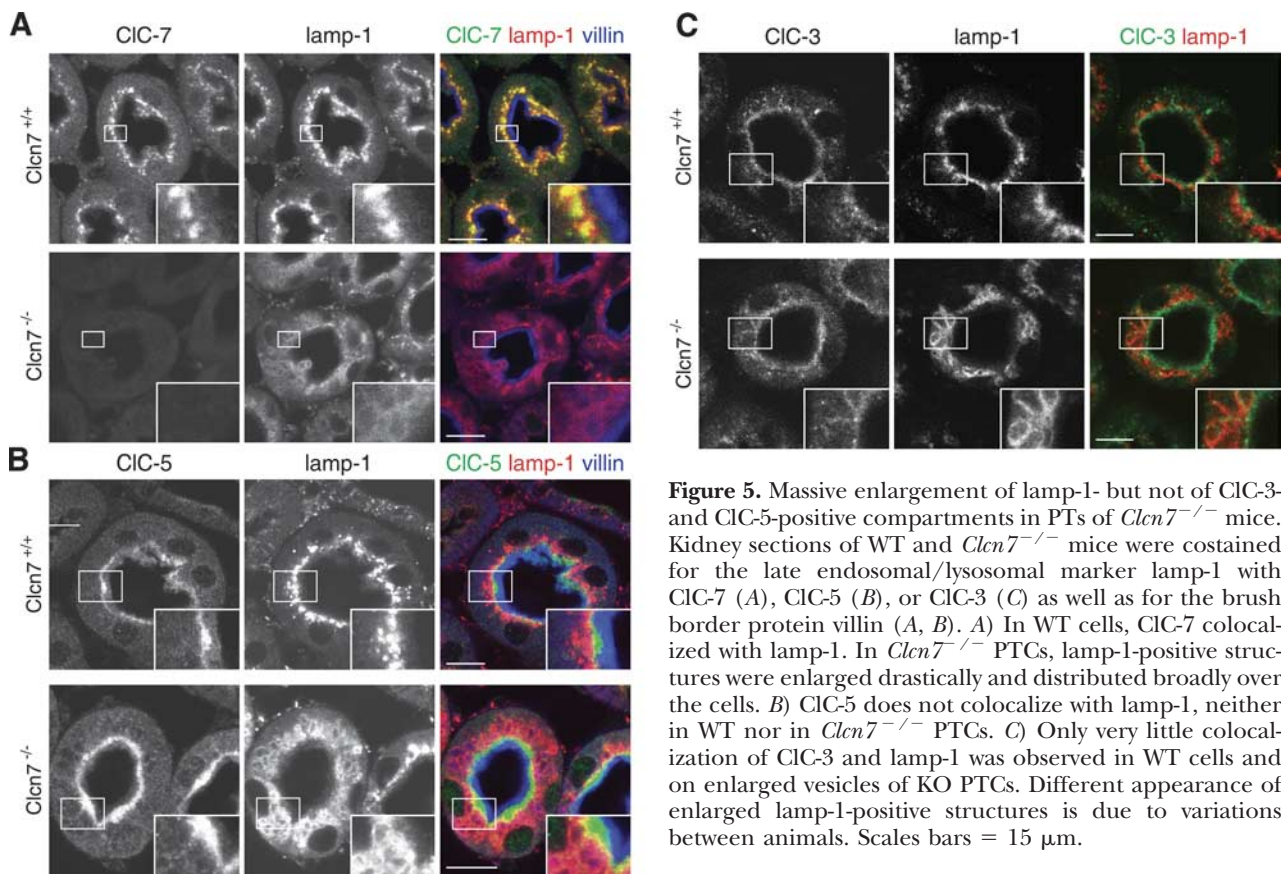
Figure 5. Massive enlargement of lamp-1- but not of ClC-3- and ClC-5-positive compartments in PTs of $Clcn7^{-/-}$ mice. Kidney sections of WT and $Clcn7^{-/-}$ mice were costained for the late endosomal/lysosomal marker lamp-1 with ClC-7 (*A*), ClC-5 (*B*), or ClC-3 (*C*) as well as for the brush border protein villin (*A*, *B*). *A*) In WT cells, ClC-7 colocalized with lamp-1. In $Clcn7^{-/-}$ PTCs, lamp-1-positive structures were enlarged drastically and distributed broadly over the cells. *B*) ClC-5 does not colocalize with lamp-1, neither in WT nor in $Clcn7^{-/-}$ PTCs. *C*) Only very little colocalization of ClC-3 and lamp-1 was observed in WT cells and on enlarged vesicles of KO PTCs. Different appearance of enlarged lamp-1-positive structures is due to variations between animals. Scales bars = 15 μm.

ciable effect on apical endocytosis. At 20 min after injection, more β-lactoglobulin fluorescence was detected in $Clcn7^{-/-}$ than WT cells of the same tubule. The same was true for 30, 40, and 60 min and 3 h (Fig. 8*A*, *B*), strongly suggesting defective degradation of endocytosed protein in ClC-7-deficient cells. Although slowed down, lysosomal degradation was not abolished completely by the loss of ClC-7, as is evident from the reduced fluorescence after 1 h of chase (Fig. 8*A*). At 24 h after injection, labeled β-lactoglobulin was absent from both WT and ClC-7-KO cells (data not shown).

To exclude that the longer half-life of β-lactoglobulin fluorescence in cells lacking ClC-7 is only due to a different handling of the fluorescent moiety, *e.g.*, owing to slowed-down exit of the dye over the lysosomal membrane, we analyzed renal degradation of labeled β-lactoglobulin by SDS-PAGE (Fig. 8*C*). Because of the early death of the global ClC-7-KO mice, we had to compare control with kidney-specific ClC-7-KO mice, even though this comparison would underestimate any effect because ClC-7 is only partially deleted. Lysates of chimeric ClC-7-KO and WT kidneys displayed a single fluorescent band with the size of uninjected labeled β-lactoglobulin at 10 min after injection (Fig. 8*C*; arrowhead), indicating that no significant lysosomal degradation of β-lactoglobulin had occurred yet. After 30 min, an additional band (Fig. 8*C*; open arrowhead), most likely a tagged β-lactoglobulin degradation product, appeared in both KO and control lysates. This band was less intense in lysates from (partial) KO kidneys. At 3 h, signals of both the undegraded protein

and the degradation product were stronger in kidney-specific ClC-7-KO than in control mice, likely because most of the β-lactoglobulin had been degraded in control mice by this time. A similar protein degradation defect was observed with injected albumin (data not shown) or with the fluid-phase endocytosis marker HRP (Supplemental Fig. 8*D*).

We next performed endocytosis/degradation experiments in chimeric ClC-5/ClC-7 double-deficient mice. At 60 min after β-lactoglobulin injection, fluorescence in PTCs lacking only ClC-7 was much stronger than in ClC-7/ClC-5 double-KO cells of the same tubule (Fig. 8*D*).

DISCUSSION

Progression of neurodegeneration and microglia activation

Like in the global ClC-7-KO, neurodegeneration in forebrain-specific ClC-7-KO mice began in the CA3 region of the hippocampus. It proceeded much further, as these mice have a normal life span. By the age of 1.5 yr, we found a nearly complete loss of neurons in the areas where ClC-7 was disrupted, whereas regions expressing ClC-7 were unaffected. This finding suggests that lysosomal storage and neurodegeneration depend on the absence of ClC-7 in a cell-autonomous manner, as we have shown stringently for lysosomal storage in the kidney. Although we could not study protein degradation in the brain as we did in the kidney, the
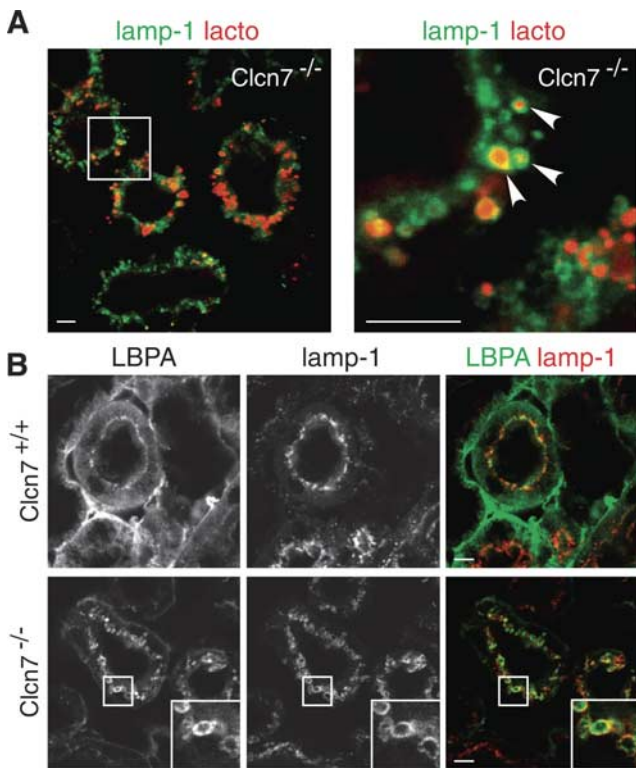
Figure 6. Enlarged lamp-1-positive structures are elements of the endocytic apparatus. *A*) A 39-d-old *Clcn7*$^{-/-}$ mouse was fixed 1 h after intravenous injection of β-lactoglobulin labeled with Alexa Fluor 546 (red). In the PTCs, endocytosed protein is present in enlarged vesicles that stain for lamp-1 (green). *B*) Kidney sections of WT and *Clcn7*$^{-/-}$ mice were costained for lamp-1 and LBPA, a marker for multivesicular bodies. Enlarged vesicles in KO cells stain for LBPA. Basolateral LBPA staining is unspecific and depends on the fixation method. Scale bars = 5 μm (*A*); 10 μm (*B*).

increase in LC3-II argues for an impairment of protein degradation in neurons also. As observed for other types of neuropathology as diverse as trauma, stroke, tumors, or neurodegenerative diseases (27, 28) and many forms of NCL (29), the neurodegeneration of ClC-7-KO mice is accompanied by massive activation of microglia and astrocytes (ref. 6 and the present study).

In forebrain-specific ClC-7-KO mice, which to our knowledge represent the first conditional KO mouse model for NCL, we found that this activation was restricted to brain regions in which ClC-7 had been deleted from neurons. In the regions and at time points where forebrain-specific and global ClC-7-KO mice could be compared, no difference in lysosomal storage, neurodegeneration, or glial activation could be detected, although activated microglia in the forebrain-specific KO mice express ClC-7. This observation suggests that the disruption of ClC-7 in glia does not play a major role in the CNS pathology of *Clcn7*$^{-/-}$ mice. It does not rule out, however, that activation of microglia contributes to the observed CNS pathology.

Renal PTs as model system

In PTCs of the kidney, different endolysosomal compartments are spatially segregated, with early endosomes localized close to the apical membrane, providing favorable conditions for studying the transport and processing of endocytosed protein. Moreover, these cells display particularly high endocytotic activity, which serves to recover protein-bound vitamins from the glomerular filtrate (30). By vascular perfusion, endocytotic substrate can be administered rapidly to the apical membrane of PTCs. This allows for unique *in vivo* pulse-chase experiments of endocytosis (11). Endocytosis can be compared quantitatively between genotypes by studying chimeric tubules in which WT and KO cells lie side by side. The X-chromosomal localization of the *Clcn5* gene allowed the generation of chimeric tubules simply by generating heterozygous females (11). We here exploited the incomplete deletion of ClC-7 in crosses of floxed mice with ApoE-cre mice (19). These kidney-specific ClC-7-KO mice also facilitate endocytosis experiments because they can be performed with adult animals. Our choice of the PT as model system is underpinned by the observation of lysosomal storage material in PTCs of *Clcn7*$^{-/-}$ or *Ostm1*$^{-/-}$ (*gray lethal*) mice (6, 8).

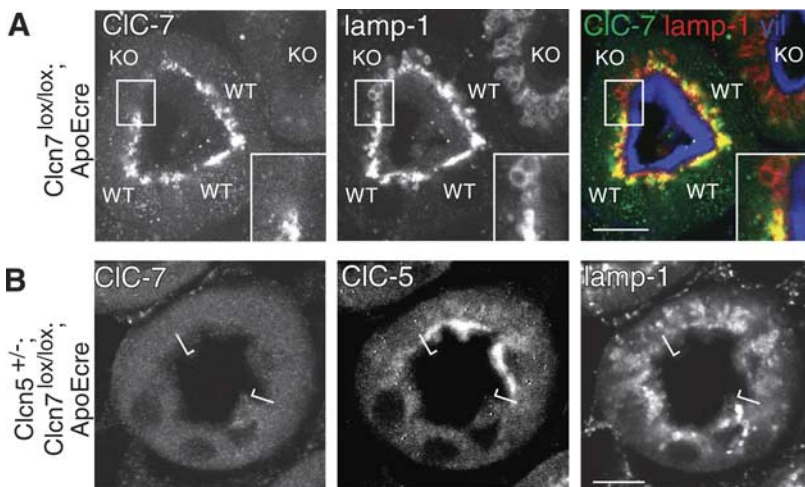Analysis of PTs from these mice gave three important

Figure 7. Decrease in endocytosis does not affect the lysosomal phenotype of ClC-7-KO PTCs. *A*) Immunostaining against ClC-7 (green) and lamp-1 (red) on PTCs of kidney-specific ClC-7-KO mice detects enlarged lamp-1-positive late endosomes-lysosomes only in ClC-7-deficient cells (KO) of a chimeric PT. *B*) Kidney sections of ClC-5/ClC-7 double-KO (*Clcn5*$^{+/-}$;*Clcn7*$^{lox/lox}$;*ApoEcre*) mice were immunostained for ClC-7, ClC-5, and lamp-1. The additional loss of ClC-5 has no discernible effect on the altered lamp-1 distribution in ClC-7-deficient cells. Brackets indicate ClC-5-expressing cells of a chimeric PT. Scale bars = 15 μm.
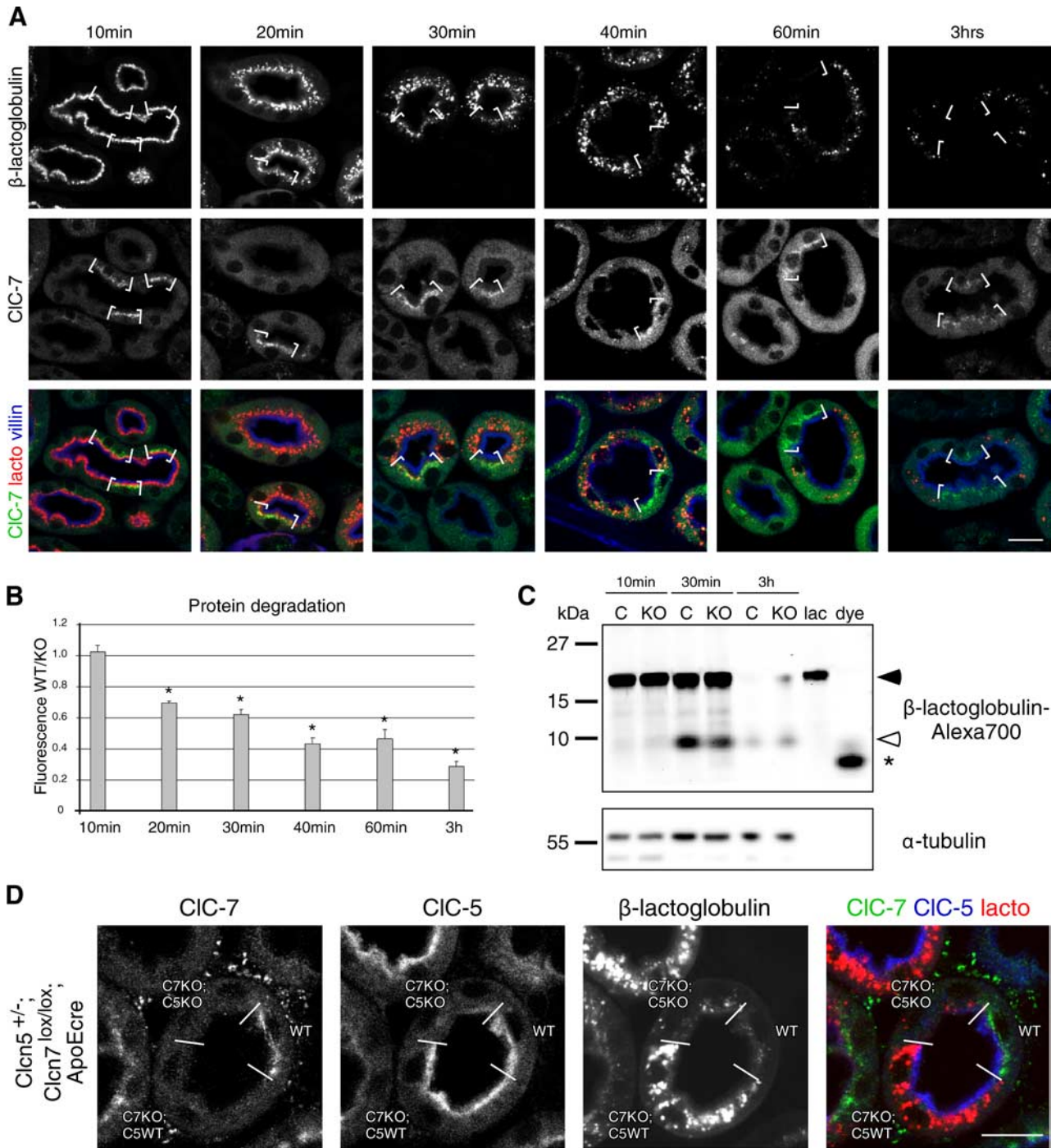
Figure 8. Lysosomal protein degradation depends on ClC-7. Kidney-specific ClC-7-KO mice (*A–C*) or ClC-5/ClC-7(kidney-specific) double-KO mice (*D*) were injected with fluorescently labeled β-lactoglobulin. *A*) Kidney sections were fixed at indicated time points and stained with anti-ClC-7 and anti-villin antibodies. Confocal microscopy showed that β-lactoglobulin fluorescence was more intense in ClC-7-KO than in WT cells (in brackets) of the same chimeric PT at time points >10 min. (Apparently stronger ClC-7 signal at 40 and 60 min caused by variations in antibody background.) *B*) At 10 min after uptake, β-lactoglobulin fluorescence in WT and ClC-7-KO cells in chimeric tubules was indistinguishable, but at later time points, fluorescence was more intense in ClC-7-KO than in WT cells (number of tubules measured: 10 min, $n=71$; 20 min, $n=157$; 30 min, $n=106$; 40 min, $n=79$; 60 min, $n=71$; 3 h, $n=95$); 3 animals/time point. Error bars = SEM. *$P < 0.0001$. *C*) SDS-PAGE analysis of kidney lysates with subsequent detection of labeled β-lactoglobulin by fluorescence (top panel) or of α-tubulin by immunoblotting (bottom panel). At 10 min after injection, almost all fluorescence migrated with the full-length β-lactoglobulin (filled arrowhead). After 30 min, fluorescence migrating below 10 kDa (open arrowhead) indicated a β-lactoglobulin degradation product that was more prominent in control (C) than in KO lysates. It migrated more slowly than the free dye (asterisk). At 3 h after injection, KO lysate displayed more of both the full-length and the degraded protein. A representative SDS-PAGE from 3 independent experiments is shown. *D*) ClC-5/ClC-7(kidney-specific) double-KO ($Clcn5^{+/-};Clcn7^{lox/lox};ApoEcre$) kidneys were fixed 60 min after injection of β-lactoglobulin (4-fold of amount in *A–C*) and immunostained for ClC-7 and ClC-5. Fluorescence signal was stronger in PTCs lacking only ClC-7 (ClC-7KO;C5WT) than in ClC-5/ClC-7 double-KO (ClC-7KO;ClC-5KO) cells. Scale bars = 20 μm.

results: *1)* The accumulation of storage material and the generation of abnormally large vesicular structures are cell-intrinsic, occurring only in cells lacking ClC-7; *2)* apical endocytotic uptake of protein does not depend appreciably on ClC-7; and *3)* ClC-7 disruption drastically slows, but does not abolish, proteolysis of endocytosed protein.

A possibly direct effect of ion composition on protein degradation

Lysosomal protein degradation depends on the activity of acidic hydrolases. The loss of certain lysosomal enzyme activities underlies several different forms of lysosomal storage disease (31). In analogy to the role of ClC-3 and ClC-5 in acidifying endosomes (21, 32) and of ClC-7 in acidifying the resorption lacuna of osteoclasts (7), ClC-7 is believed to help in late endosomal/lysosomal acidification by shunting electric currents of the H^+-ATPase (2, 7). Thus, slower protein degradation in ClC-7-KO cells might reflect a lowered activity of acidic hydrolases caused by an elevated luminal pH. During the transport to lysosomes, prelysosomal compartments might be acidified at a slower rate. Steady-state lysosomal pH of cultured neurons or fibroblasts derived from WT, $Clcn7^{-/-}$, or $Ostm1^{-/-}$ mice, however, was undistinguishable by ratiometric fluorescence measurement (6, 8). By contrast, a recent report asserted that lysosomal pH of HeLa cells became more alkaline when ClC-7 was partially knocked down (9). However, that study used only single antisense and control siRNAs to manipulate ClC-7 levels. Disconcertingly, lysosomal pH reportedly was more acidic with the negative control than in untreated cells. Moreover, that study used nonratiometric measurements of total lysotracker fluorescence, which is not only a function of vesicular pH, but also of the number and volumes of vesicles. These latter parameters were not determined (9).

In addition to luminal pH, lysosomal chloride concentration might influence lysosomal protein degradation (2, 33, 34). For instance, there might be (so far unknown) chloride-coupled transporters for degradation products in lysosomal membranes. Chloride may also influence the activity of degradation enzymes, as shown for the lysosomal protease cathepsin C (33). Like other vesicular CLCs (4, 5), ClC-7 has been suggested to function as a Cl^-/H^+ exchanger (2, 9), with a likely stoichiometry of $2Cl^-/1H^+$. The large inside-out H^+ gradient across lysosomal membranes predicts a steady-state lysosomal Cl^- accumulation that would be reduced in ClC-7-KO cells even in the presence of unchanged lysosomal pH. Likewise, AtClC-a accumulates nitrate, an important plant nutrient, in vacuoles of *Arabidopsis thaliana* (35). Impaired protein degradation, whether owed to changed chloride or pH in (or on the way to) lysosomes, might lead to the observed enlarged lamp1-positive structures.

Trafficking defect upon ClC-7 deficiency

To investigate whether the generation of large lamp-1-positive vesicles in $Clcn7^{-/-}$ cells depends on the accumulation of undegraded endocytic cargo, we studied PTCs lacking both ClC-7 and ClC-5. Despite the strong impairment of endocytosis caused by ClC-5 disruption (11, 13, 36), similar enlarged vesicles were observed in double-KO cells. ClC-5, however, is not only crucial for the lysosomal delivery of substrate for degradation, but also of lysosomal degradative enzymes (37). Therefore, the additional loss of ClC-5 may further impair lysosomal degradation in $Clcn7^{-/-}$ cells, rendering predictions on cargo accumulation difficult. Our *in vivo* endocytosis/degradation assay shows that after a 1 h chase, ClC-5/ClC-7 double-KO cells contained much less tagged protein than $Clcn7^{-/-}$ cells, with fluorescence levels being similar to WT. We conclude that the accumulation of undegraded cargo is unlikely to be a major factor in the generation of those abnormal vesicles.

Although endocytosed protein reached those lamp-1-positive structures after a 1-h chase, those enlarged vesicles do not necessarily represent lysosomes, since lamp-1 is also present on late endosomes. Indeed, those vesicles were also positive for LBPA, a lipid enriched in multivesicular endosomes (23). This observation suggests a vesicular trafficking defect, which could also affect the delivery of degradative enzymes. PTCs may be particularly vulnerable in this respect, because of a prominent role of apical endocytosis in delivering certain proteolytic enzymes to lysosomes (37). This difference in lysosomal enzyme trafficking might explain the apparent discrepancy between the present observation of impaired proteolysis and our previous finding that the activity of the lysosomal enzyme TPP I was normal in cultured $Clcn7^{-/-}$ neurons and fibroblasts (6). Alternatively, TPP I plays no important role in the degradative pathways observed here.

A vesicular trafficking defect might also resolve the conundrum that the KO of ClC-7 abolished the acidification of the osteoclast resorption lacuna (7) but did not change lysosomal steady-state pH (6, 8). Indeed, the acid-secreting ruffled border membrane of osteoclasts, which is formed by the exocytotic insertion of lysosomal membranes, was underdeveloped in $Clcn7^{-/-}$ mice (7). Similar to the role of ClC-5 in renal endocytosis (11, 36), the loss of ClC-7 might affect intracellular trafficking by a reduced acidification rate of late endosomes. The recruitment of some components of the vesicular transport machinery is pH-sensitive (38–40), and transport between various compartments of the endocytic pathway depends on vesicular H^+-ATPase activity (41, 42). So far, no role of chloride in membrane trafficking is known apart from its indirect role in supporting vesicular acidification. However, novel roles of vesicular chloride are emerging. For instance, a recent report described the regulation of an early endosomal Ca^{2+} channel by luminal $[Cl^-]$ (43). Some evidence indicates that the

release of vesicular Ca^{2+} affects vesicle fusion and trafficking (44).

Relationship to other CLCs

The existence of 5 distinct vesicular CLC proteins in the endosomal-lysosomal pathway (ClC-3 through ClC-7) raises the possibility of a partial compensation of the loss of ClC-7 by other CLCs. Although the localization of different vesicular CLC transporters has been studied by immunocytochemistry in transfected cells (26) and by subcellular fractionation of native tissues (6), no costaining of different endogenous intracellular CLC proteins has been available. Our results show that the majority of ClC-5- or ClC-3-positive endosomes is distinct from ClC-7-positive late endosomes/lysosomes, agreeing with their localization to earlier endocytotic compartments (2). We have observed previously that a proportion of ClC-3 and ClC-6 moved toward denser, lysosome-containing fractions in brain lysates of ClC-7-KO mice (45). We have found in this work that the expression level and distribution of ClC-5 was unchanged by the loss of ClC-7 and that enlarged lamp-1-positive late endosomes/lysosomes of ClC-7-KO PTCs did not stain for ClC-5. Both in WT and in ClC-7-KO mice, we found a minor overlap of ClC-3 staining with lamp-1, as shown previously on "normal" lamp-1-positive structures in transfected cells (14). The localization of ClC-3, which showed unaltered expression levels, seemed to be largely unchanged by ClC-7 disruption. The only other late endosomal CLC protein, ClC-6, is not expressed in the kidney (45). Therefore, a major compensatory effect of ClC-5 or ClC-3 on lysosomal protein degradation in ClC-7-KO PTCs can be excluded.

CONCLUSIONS

Using a novel floxed ClC-7 mouse model, we have demonstrated for the first time that the lysosomal chloride transporter ClC-7/Ostm1 is important for the degradation of endocytosed protein, at least in the kidney. The failure to degrade endocytosed proteins adequately may lead to the lysosomal storage disease observed in mice and humans lacking this chloride transport activity. FJ

REFERENCES

1. Brandt, S., and Jentsch, T. J. (1995) ClC-6 and ClC-7 are two novel broadly expressed members of the CLC chloride channel family. *FEBS Lett.* **377,** 15–20
2. Jentsch, T. J. (2007) Chloride and the endosomal-lysosomal pathway: emerging roles of CLC chloride transporters. *J. Physiol.* **578,** 633–640
3. Accardi, A., and Miller, C. (2004) Secondary active transport mediated by a prokaryotic homologue of ClC Cl- channels. *Nature* **427,** 803–807
4. Picollo, A., and Pusch, M. (2005) Chloride/proton antiporter activity of mammalian CLC proteins ClC-4 and ClC-5. *Nature* **436,** 420–423
5. Scheel, O., Zdebik, A. A., Lourdel, S., and Jentsch, T. J. (2005) Voltage-dependent electrogenic chloride/proton exchange by endosomal CLC proteins. *Nature* **436,** 424–427
6. Kasper, D., Planells-Cases, R., Fuhrmann, J. C., Scheel, O., Zeitz, O., Ruether, K., Schmitt, A., Poët, M., Steinfeld, R., Schweizer, M., Kornak, U., and Jentsch, T. J. (2005) Loss of the chloride channel ClC-7 leads to lysosomal storage disease and neurodegeneration. *EMBO J.* **24,** 1079–1091
7. Kornak, U., Kasper, D., Bösl, M. R., Kaiser, E., Schweizer, M., Schulz, A., Friedrich, W., Delling, G., and Jentsch, T. J. (2001) Loss of the ClC-7 chloride channel leads to osteopetrosis in mice and man. *Cell* **104,** 205–215
8. Lange, P. F., Wartosch, L., Jentsch, T. J., and Fuhrmann, J. C. (2006) ClC-7 requires Ostm1 as a beta-subunit to support bone resorption and lysosomal function. *Nature* **440,** 220–223
9. Graves, A. R., Curran, P. K., Smith, C. L., and Mindell, J. A. (2008) The Cl-/H+ antiporter ClC-7 is the primary chloride permeation pathway in lysosomes. *Nature* **453,** 788–792
10. Mellman, I., Fuchs, R., and Helenius, A. (1986) Acidification of the endocytic and exocytic pathways. *Annu. Rev. Biochem.* **55,** 663–700
11. Piwon, N., Günther, W., Schwake, M., Bösl, M. R., and Jentsch, T. J. (2000) ClC-5 Cl- -channel disruption impairs endocytosis in a mouse model for Dent's disease. *Nature* **408,** 369–373
12. Lloyd, S. E., Pearce, S. H., Fisher, S. E., Steinmeyer, K., Schwappach, B., Scheinman, S. J., Harding, B., Bolino, A., Devoto, M., Goodyer, P., Rigden, S. P., Wrong, O., Jentsch, T. J., Craig, I. W., and Thakker, R. V. (1996) A common molecular basis for three inherited kidney stone diseases. *Nature* **379,** 445–449
13. Wang, S. S., Devuyst, O., Courtoy, P. J., Wang, X. T., Wang, H., Wang, Y., Thakker, R. V., Guggino, S., and Guggino, W. B. (2000) Mice lacking renal chloride channel, CLC-5, are a model for Dent's disease, a nephrolithiasis disorder associated with defective receptor-mediated endocytosis. *Hum. Mol. Genet.* **9,** 2937–2945
14. Stobrawa, S. M., Breiderhoff, T., Takamori, S., Engel, D., Schweizer, M., Zdebik, A. A., Bösl, M. R., Ruether, K., Jahn, H., Draguhn, A., Jahn, R., and Jentsch, T. J. (2001) Disruption of ClC-3, a chloride channel expressed on synaptic vesicles, leads to a loss of the hippocampus. *Neuron* **29,** 185–196
15. Chalhoub, N., Benachenhou, N., Rajapurohitam, V., Pata, M., Ferron, M., Frattini, A., Villa, A., and Vacher, J. (2003) Grey-lethal mutation induces severe malignant autosomal recessive osteopetrosis in mouse and human. *Nat. Med.* **9,** 399–406
16. Frattini, A., Pangrazio, A., Susani, L., Sobacchi, C., Mirolo, M., Abinun, M., Andolina, M., Flanagan, A., Horwitz, E. M., Mihci, E., Notarangelo, L. D., Ramenghi, U., Teti, A., Van Hove, J., Vujic, D., Young, T., Albertini, A., Orchard, P. J., Vezzoni, P., and Villa, A. (2003) Chloride channel ClCN7 mutations are responsible for severe recessive, dominant, and intermediate osteopetrosis. *J. Bone Miner. Res.* **18,** 1740–1747
17. Pangrazio, A., Poliani, P. L., Megarbane, A., Lefranc, G., Lanino, E., Di Rocco, M., Rucci, F., Lucchini, F., Ravanini, M., Facchetti, F., Abinun, M., Vezzoni, P., Villa, A., and Frattini, A. (2006) Mutations in OSTM1 (grey lethal) define a particularly severe form of autosomal recessive osteopetrosis with neural involvement. *J. Bone Miner. Res.* **21,** 1098–1105
18. Iwasato, T., Datwani, A., Wolf, A. M., Nishiyama, H., Taguchi, Y., Tonegawa, S., Knopfel, T., Erzurumlu, R. S., and Itohara, S. (2000) Cortex-restricted disruption of NMDAR1 impairs neuronal patterns in the barrel cortex. *Nature* **406,** 726–731

19. Leheste, J. R., Melsen, F., Wellner, M., Jansen, P., Schlichting, U., Renner-Muller, I., Andreassen, T. T., Wolf, E., Bachmann, S., Nykjaer, A., and Willnow, T. E. (2003) Hypocalcemia and osteopathy in mice with kidney-specific megalin gene defect. *FASEB J.* **17,** 247–249

20. Schwenk, F., Baron, U., and Rajewsky, K. (1995) A Cre-transgenic mouse strain for the ubiquitous deletion of loxP-flanked gene segments including deletion in germ cells. *Nucl. Acids Res.* **23,** 5080–5081

21. Günther, W., Luchow, A., Cluzeaud, F., Vandewalle, A., and Jentsch, T. J. (1998) ClC-5, the chloride channel mutated in Dent's disease, colocalizes with the proton pump in endocytotically active kidney cells. *Proc. Natl. Acad. Sci. U. S. A.* **95,** 8075–8080

22. Maritzen, T., Keating, D. J., Neagoe, I., Zdebik, A. A., and Jentsch, T. J. (2008) Role of the vesicular chloride transporter ClC-3 in neuroendocrine tissue. *J. Neurosci.* **28,** 10587–10598

23. Kobayashi, T., Stang, E., Fang, K. S., de Moerloose, P., Parton, R. G., and Gruenberg, J. (1998) A lipid associated with the antiphospholipid syndrome regulates endosome structure and function. *Nature* **392,** 193–197

24. Rubinsztein, D. C., Cuervo, A. M., Ravikumar, B., Sarkar, S., Korolchuk, V., Kaushik, S., and Klionsky, D. J. (2009) In search of an "autophagomometer." *Autophagy* **5,** 585–589

25. Estévez, R., Boettger, T., Stein, V., Birkenhäger, R., Otto, E., Hildebrandt, F., and Jentsch, T. J. (2001) Barttin is a Cl- channel beta-subunit crucial for renal Cl- reabsorption and inner ear K+ secretion. *Nature* **414,** 558–561

26. Suzuki, T., Rai, T., Hayama, A., Sohara, E., Suda, S., Itoh, T., Sasaki, S., and Uchida, S. (2006) Intracellular localization of ClC chloride channels and their ability to form hetero-oligomers. *J. Cell. Physiol.* **206,** 792–798

27. Kreutzberg, G. W. (1996) Microglia: a sensor for pathological events in the CNS. *Trends Neurosci.* **19,** 312–318

28. Pekny, M., and Nilsson, M. (2005) Astrocyte activation and reactive gliosis. *Glia* **50,** 427–434

29. Cooper, J. D., Russell, C., and Mitchison, H. M. (2006) Progress towards understanding disease mechanisms in small vertebrate models of neuronal ceroid lipofuscinosis. *Biochim. Biophys. Acta.* **1762,** 873–889

30. Christensen, E. I., and Birn, H. (2002) Megalin and cubilin: multifunctional endocytic receptors. *Nat. Rev. Mol. Cell. Biol.* **3,** 256–266

31. Gieselmann, V. (1995) Lysosomal storage diseases. *Biochim. Biophys. Acta.* **1270,** 103–136

32. Hara-Chikuma, M., Yang, B., Sonawane, N. D., Sasaki, S., Uchida, S., and Verkman, A. S. (2005) ClC-3 chloride channels facilitate endosomal acidification and chloride accumulation. *J. Biol. Chem.* **280,** 1241–1247

33. Cigič, B., and Pain, R. H. (1999) Location of the binding site for chloride ion activation of cathepsin C. *Eur. J. Biochem.* **264,** 944–951

34. Faundez, V., and Hartzell, H. C. (2004) Intracellular chloride channels: determinants of function in the endosomal pathway. *Sci. STKE* 2004, re8

35. De Angeli, A., Monachello, D., Ephritikhine, G., Frachisse, J. M., Thomine, S., Gambale, F., and Barbier-Brygoo, H. (2006) The nitrate/proton antiporter AtCLCa mediates nitrate accumulation in plant vacuoles. *Nature* **442,** 939–942

36. Günther, W., Piwon, N., and Jentsch, T. J. (2003) The ClC-5 chloride channel knock-out mouse—an animal model for Dent's disease. *Pflügers Arch.* **445,** 456–462

37. Nielsen, R., Courtoy, P. J., Jacobsen, C., Dom, G., Lima, W. R., Jadot, M., Willnow, T. E., Devuyst, O., and Christensen, E. I. (2007) Endocytosis provides a major alternative pathway for lysosomal biogenesis in kidney proximal tubular cells. *Proc. Natl. Acad. Sci. U. S. A.* **104,** 5407–5412

38. Aniento, F., Gu, F., Parton, R. G., and Gruenberg, J. (1996) An endosomal beta COP is involved in the pH-dependent formation of transport vesicles destined for late endosomes. *J. Cell Biol.* **133,** 29–41

39. Zeuzem, S., Feick, P., Zimmermann, P., Haase, W., Kahn, R. A., and Schulz, I. (1992) Intravesicular acidification correlates with binding of ADP-ribosylation factor to microsomal membranes. *Proc. Natl. Acad. Sci. U. S. A.* **89,** 6619–6623

40. Maranda, B., Brown, D., Bourgoin, S., Casanova, J. E., Vinay, P., Ausiello, D. A., and Marshansky, V. (2001) Intra-endosomal pH-sensitive recruitment of the Arf-nucleotide exchange factor ARNO and Arf6 from cytoplasm to proximal tubule endosomes. *J. Biol. Chem.* **276,** 18540–18550

41. Clague, M. J., Urbe, S., Aniento, F., and Gruenberg, J. (1994) Vacuolar ATPase activity is required for endosomal carrier vesicle formation. *J. Biol. Chem.* **269,** 21–24

42. Van Weert, A. W., Dunn, K. W., Gueze, H. J., Maxfield, F. R., and Stoorvogel, W. (1995) Transport from late endosomes to lysosomes, but not sorting of integral membrane proteins in endosomes, depends on the vacuolar proton pump. *J. Cell Biol.* **130,** 821–834

43. Saito, M., Hanson, P. I., and Schlesinger, P. (2007) Luminal chloride-dependent activation of endosome calcium channels: patch clamp study of enlarged endosomes. *J. Biol. Chem.* **282,** 27327–27333

44. Luzio, J. P., Bright, N. A., and Pryor, P. R. (2007) The role of calcium and other ions in sorting and delivery in the late endocytic pathway. *Biochem. Soc. Trans.* **35,** 1088–1091

45. Poët, M., Kornak, U., Schweizer, M., Zdebik, A. A., Scheel, O., Hoelter, S., Wurst, W., Schmitt, A., Fuhrmann, J. C., Planells-Cases, R., Mole, S. E., Hübner, C. A., and Jentsch, T. J. (2006) Lysosomal storage disease upon disruption of the neuronal chloride transport protein ClC-6. *Proc. Natl. Acad. Sci. U. S. A.* **103,** 13854–13859